1 Results of SNR Simulations

1.1 General Properties of the SNR Simulations

This section describes the simulation results with respect to the typical phases an evolution of SRN passes through.

All existing models of a SNR exhibit qualitatively similar evolution. We illustrate this evolution in Figure 11. The three panels show (from left to right, respectively) the simulation beginning, the Sedov-Taylor phase, and the Pressure-Driven-Shell phase. We see how the initial small sphere of the extremely hot gas evolves to the swept-up shell of hot ISM, with density, temperature and pressure following the typical Sedov profiles, which later collapses into a thin shell.

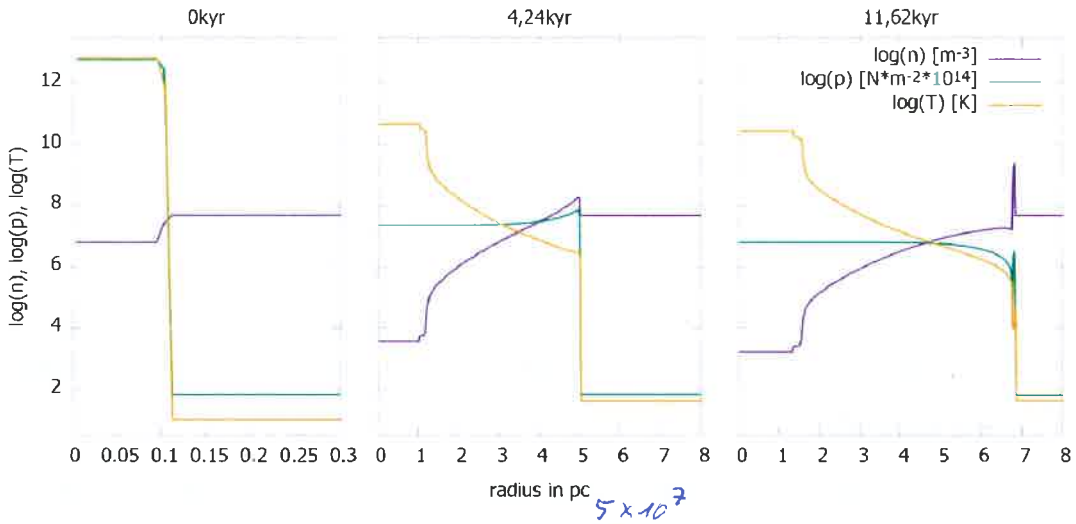

Fig. 1 Three stages of SNR evolving in the gas with density of ~~5E7~~ particles per cubic ~~centi~~metre using Schure cooling module. The radial profiles of the density (violet), pressure (blue), and temperature (yellow) are shown with the time of the stage denoted above each panel.

The ~~first graph~~ shows the initial ~~values at the beginning~~. Of particular interest is the high value of the pressure and temperature in comparison to the ~~ISM~~. The second ~~graph~~, in turn, depicts the same remnant during the Sedov-Taylor phase. The shape of the function between about 2 to 5 parsecs is ~~very similar~~ to the ideal Sedov-Taylor solution shown in Fig. 3 in Chapter 3. The ~~third graph~~ shows the remnant shortly after the shell collapse, during the Pressure-Driven-Shell phase. Especially interesting is the abrupt change in density at the shock front. It changes by a factor of $\lesssim 4$ in the Sedov-Taylor phase, which is a fundamental property of the adiabatic shock. At the same time, the density jump is much higher in the Pressure-Driven-Shell phase in the third graph, because the shock is losing the energy through radiation, i.e. it is a radiative shock and not an adiabatic shock.

Also of interest is the function describing the radius of the shock front as it varies with time, represented by the output of the t_shell code. Fig 12 illustrates this relationship with the same ISM density as in the previous Fig 11. Notably, the change in the growth rate appears at approximately $6\,kyr$, which marks the transition from the Sedov-Taylor phase to the Pressure-Driven-Shell phase.

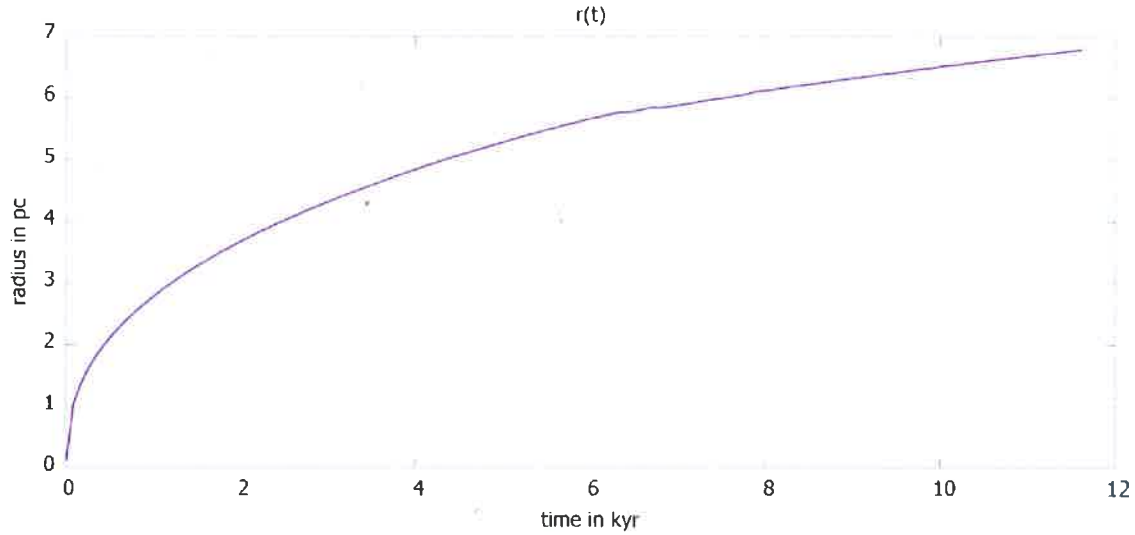

Fig. 2 The radius of the shock front as a function of time of the same SNR as the one shown in Fig. 11.

1.2 Comparison Between the Simulations with the Schure vs. Chemistry Cooling modules

Both simulations generally follow the expected development of a SNR evolution. At the same time, differences between the two simulations were observed starting with the shell collapse, i.e. the transition from the Sedov-Taylor to the Pressure-Driven-Shell phase. This critical comparison is displayed in Fig. 13 which shows the time of the shell collapse, as a function of the ISM density for the simulation with the Schure cooling module (blue) and the chemistry module (red). The dots represent the observed shell collapses in simulations, while the lines represent a power-law fit.

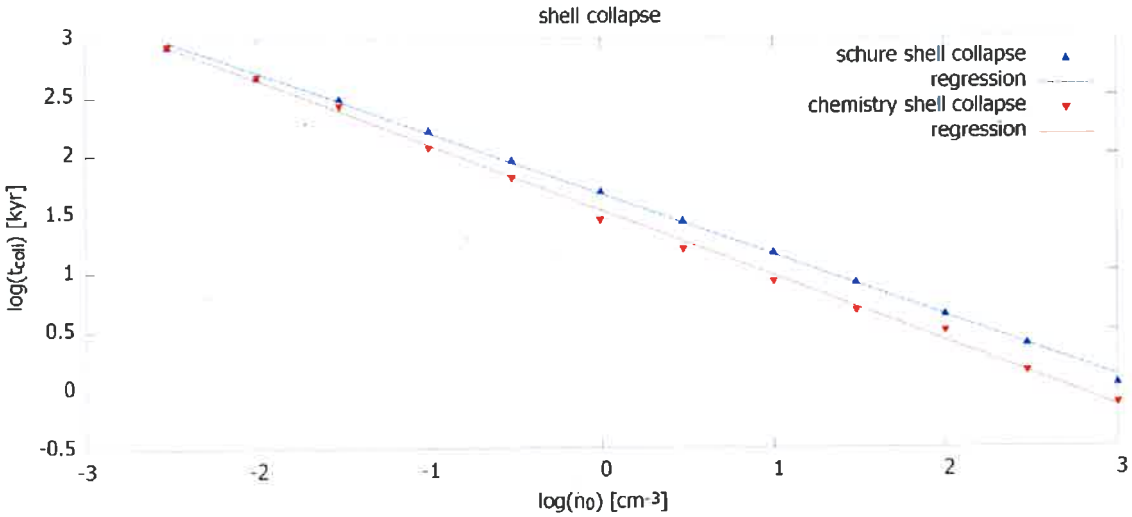

Fig. 3 The shell collapse time as a function of the ISM density. The blue dots represent the collapse according to the Schure cooling module while the red dots represent the chemistry cooling module.

As evident in Fig. 13, there are discernible differences between the Schure cooling module and the chemistry cooling module between how fast their shell collapse. The SNR simulated with the chemistry cooling module collapses ~~more rapidly~~, especially at higher densities, whereas it collapses nearly simultaneously with the Schure cooling at lower densities.

Fig. 14 ~~displays~~ the same phenomenon, ~~but includes the expansion of the different simulations over time, using a logarithmic scale, allowing for a better comparison of both cooling modules.~~

by showing shell radii as functions of time in the logarithmic scale for all the simulations.

- add to the next paragraph

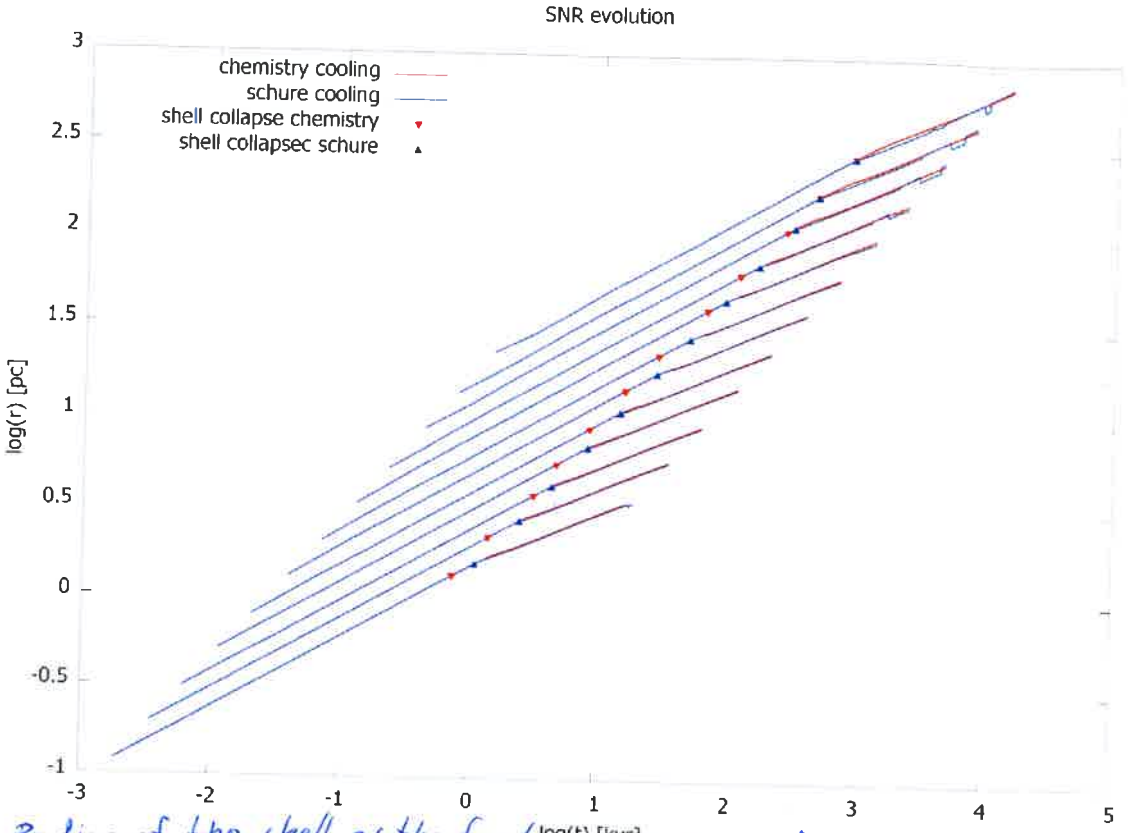

Radius of the shell as the function of time for all the simulations with

Fig. 7. The chemistry cooling module and the Schure cooling module.

The red and blue triangles represent the points of shell collapses of chemistry and Schure cooling respectively. The first observation is that the evolution of the SNRs simulated using the two cooling modules remains ~~nearly~~ identical until the shell collapse as detected in the Schure cooling module simulations (the blue and the red lines overlap up to the blue triangles). However, our predictions suggested that the evolution should diverge earlier, specifically at the earlier of the two collapses, in this case the collapse of the chemistry cooling module (red triangles).

Upon further investigation, it became apparent that before the shell of the chemistry cooling module collapses (red triangle), the density at the shock front begins to spike and surpasses the threshold of the $\lesssim 4$ times of the ISM density. This is demonstrated in detail in Fig. 15- the spike is the top of the red curve representing the simulation with the chemistry module. The density spike appears prior to the actual collapse, causing the observed discrepancy between our predictions and the simulations results. It also explains the differences observed in the shell collapses between the Schure and chemistry modules, as depicted in Fig. 13 and Fig. 14.

Very good !

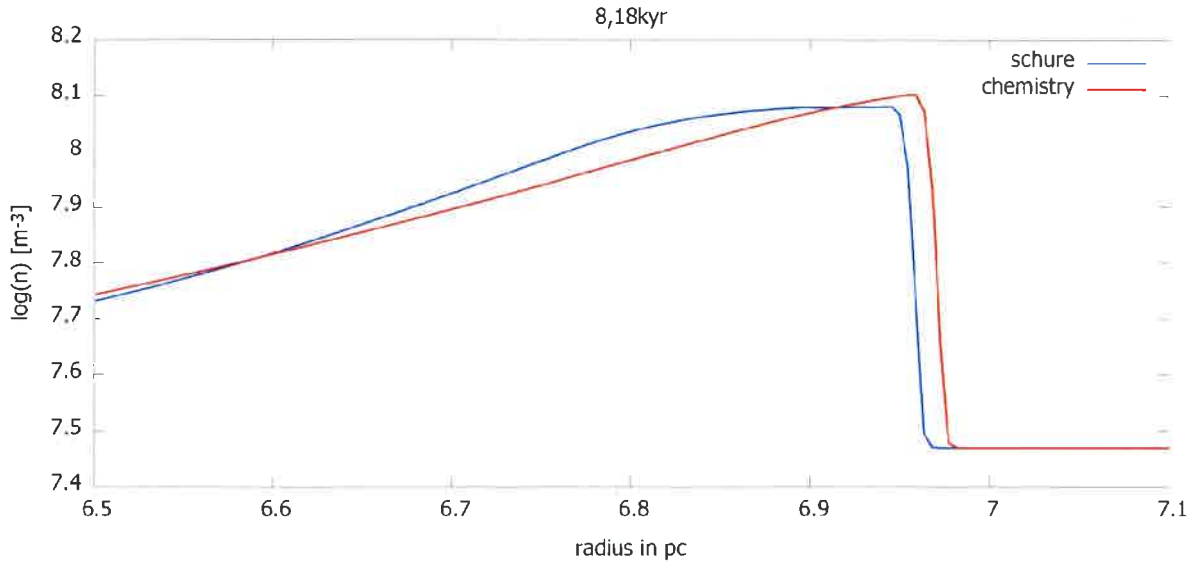

Fig. 5 The density at the shock front during the end of the Sedov-Taylor Phase as calculated by the Schure module (blue line) and by the chemistry module (red line). These simulations have a density ~~multiplier of 30~~ 3 x 10⁷ particles per cubic meter, the ambient gas

Figure 15 shows how the cooling modules treat the increase of mass at the shock front, right before their collapse, in comparison. As explained above, the chemistry module stays true to the shape of the Sedov-Taylor Solution by increasing the density at the shock front. However, by doing so, it surpasses the threshold of the $\lesssim 4$ times of the ISM density and thus deviates from the ideal Sedov-Taylor solution in this aspect. Because it surpasses this threshold, the code used to detect the shell collapse returns a true statement, even though the shell did not collapse yet.

On the other hand, in the simulation with the Schure cooling module ~~solves the same problem by adding the mass~~ the density grows further behind the shock front causing it to bulge out. The Schure cooling thus deviates from the ideal shape of the Sedov-Taylor solution shown in Fig. 3. However, it does not cross the critical threshold of the $\lesssim 4$ times of the ISM density at the shock front.

Fig. 14 demonstrates also another difference between the simulations with the two cooling modules. It can be observed during the later stages of the Pressure-Driven-Shell phase of the SNRs simulated using low density ISM (top right). There the Schure cooling module simulation exhibits occasional abrupt changes in its radius. Further investigation focused on explanation of these irregularities (see Fig. 16).

Analysing a mechanism, either physical or numerical, leading to the formation of the additional spike is beyond the scope of this work.

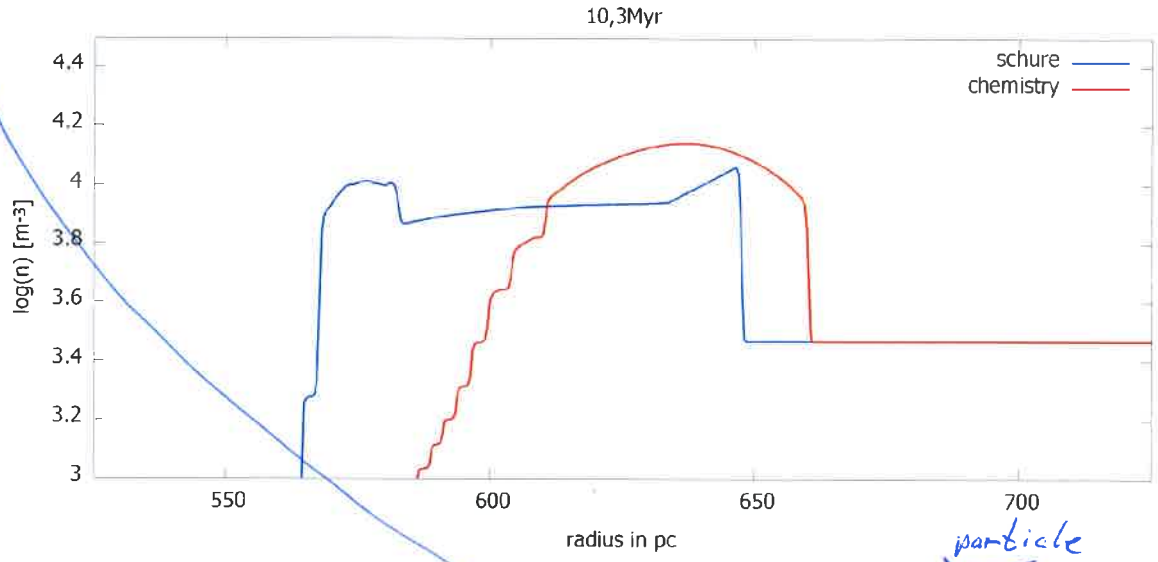

particle

Fig. 6 The density as a function of radius of the shock front of a low ISM density SNR, with an ISM density ~~multiplier of~~ 0.003. The blue line represents the SNRs evolution according to the Schure module, while the red line predicts it according to the chemistry module.

m-3

The cause for the irregularities observed in Fig. 14 turned out to be the density spike of the Schure cooling module that appears at about 570 parsecs as displayed in Fig. 16. This additional first spike was sometimes detected by the code and interpreted as the radius of the SNR since it occasionally surpassed the actual shock front in density. The chemistry module does not produce additional density spikes, since its density distribution is shaped like a cone.

Barring these two differnces, the two cooling modules exhibit ~~surprisingly~~ remarkably similar behaviour.

2 Comparison to the Catalogue data

The catalogue "Galactic SNRs: Summary Data" is used in this work to assess basic information about various SNRs. It was used alongside data reported by other researchers to be compared with the simulations results. Out of the 303 SNRs in the catalogue, only ten contain the complete set of required information for this study, including age, size, and distance. However, even within these ten SNRs, not all data necessarily has to be accurate. For example, in the case of Cassiopeia A, it is unclear whether it can be attributed to the specific SN explosion in the late 17th century, or not.

When available, the catalogue provides the year of the explosion, the SNR diameter (l), in arcminutes, and the estimated distance to the SNR (d) in kiloparsecs (kpc). The age of the SNR is calculated as the time difference between the SN and 2022, the year of the catalogue's most recent update. The radius of the SNR in centimetres is computed using the formula:

If d is given in kpc and l in arcmin, r_{SN} is set in pc with a factor 0.145 resulting from the unit conversion.

$$r_{SN} = \frac{1}{2} \cdot d \cdot l = 0{,}145 \left(\frac{d}{kpc} \right) \cdot \left(\frac{l}{arcmin} \right) pc$$

Here, d represents the distance ~~in kpc~~ and l represents the angular diameter of the SNR ~~in arcmin.~~ ~~The multiplier of 0,145 pc was derived from the units kpc and arcmin~~. To note is also the substantial uncertainty associated with most distance measurements. In this work, the average of all distances given by the catalogue were used. The following Table 1 presents the relevant properties of the 10 SNRs from the catalogue that fulfilled the criteria, as well as parameters calculated using them.

corresponding SN	size in arcmin	distance in kpc	location in galactic coordinates	alternate names	age in years	radius in pc
AD 0185	35	4,1	G320,4-1,2	RCW 86	1837	20,8
AD 0185	42	2,1	G315,4-2,3	RCW 89	1837	13,7
AD 0386	22	4,6	G11,2-0,3	/	1636	14,7
AD 1006	30	1,9	G327,6+14,6	/	1016	8,3
AD 1052	6	2,0	G184.6-5,8	Crab Nebula	970	1,7
AD 1181	7	2,0	G130,7+3,1	/	841	2,0
AD 1408	80	3,1	G69,0+2,7	CTB 80	614	36,0
AD 1572	8	2,5	G120,1+1,4	Tycho	450	2,9
AD 1604	3	3,9	G4,5+6,8	Kepler	418	1,7
~AD 1690	5	3,1	G111,7-2,1	Cassiopeia A	~332	2,2
/	7	6,1	G74,9+1,2	CTB 87	9000	6,2
/	8	3,8	G63,7+1,1	/		4,4pc

Table 1 The SNe, as well as the data received from the catalogue of all the SNe, where a size, distance and age were given.

Table 2 comprises the density ϱ_0 of the ISM of five of the 10 SNRs that were available for looking up in additional literature.

SNR	density	Literature
AD 0185	0,001	Broersen et al. 2018
AD 1006	0,05	Acero et al. 2017

AD 1052	2,5	Wallace et al. 1999
AD 1690	2,1	Fesen et al. 2016
G74,9+1,2	0,2	Matheson et al. 2013

Table 2 The SNe of Table 1 where their ISM density could be found, as well as their density and the literature it was found in.

simulations

For a comprehensive comparison between the ~~cooling modules~~ and the catalogue data, the graph presented in Fig. 17 displays the evolution of the Schure cooling, alongside SNRs listed in the catalogue. The x-axis represents time, the y-axis represents radius, and the color-coding signifies the ISM density for both simulations and SNRs. SNRs depicted in grey indicate instances where the ISM density remains undetermined.

or SNR age

the SNR

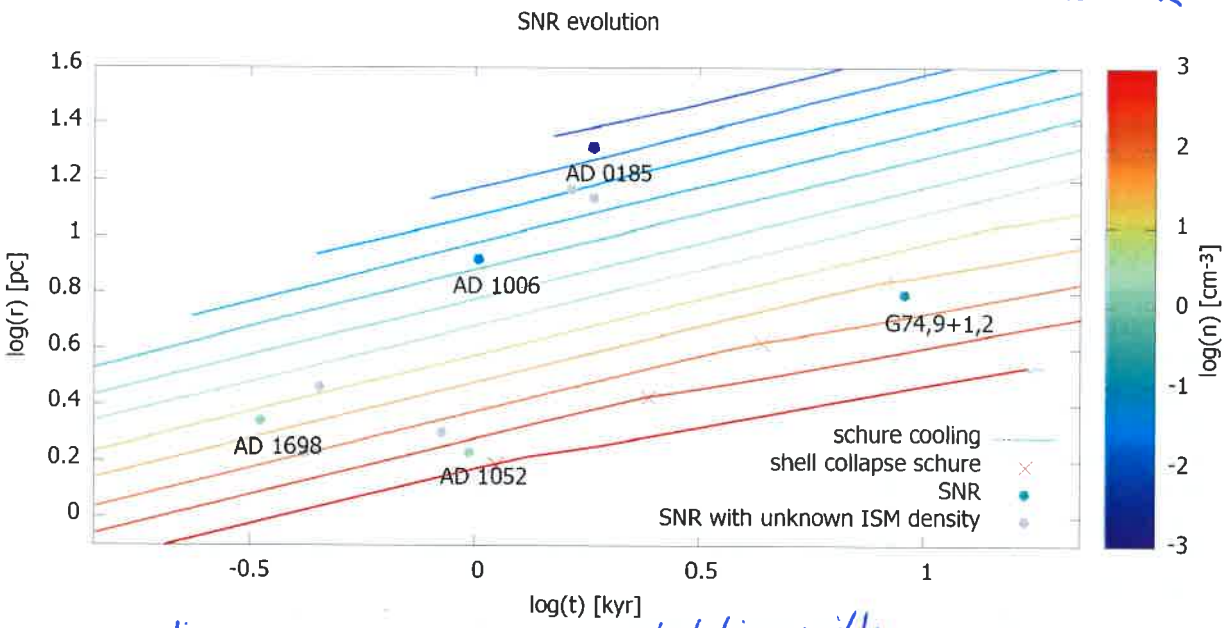

radius

calculations with

Fig. 7 The ~~size~~ of the SNR as a function of time. This graph only shows the Schure cooling module. ~~However, it also shows~~ the SNR from literature data. The colour indicates the ISM density.

and compares them to

Both SNR AD 0185 and AD 1006 exhibit a strong correlation with the simulation results. However, SNR AD 1698 appears to deviate slightly, roughly by about half a dex from the simulation data. In contrast, SNR AD 1052 and G74.9+1.2 show a significant discrepancy when compared to the simulations. Unfortunately, due to limited available data, particularly concerning ISM density, ~~Figure 15~~ is restricted to only five SNRs.

the comparison

The limited external data and the large uncertainty associated with it make it impossible to arrive at a definitive assessment of the results. This challenge is compounded by the fact that the SNRs examined in the literature data represent unique cases ~~with interesting properties and do not necessarily correspond to typical SNRs, as they otherwise would not be examined~~

for which the determination of the ambient density was possible. It is generally very difficult, another complication is that the ISM in which the SNR evolves is almost never uniform,

as it is reshaped by the stellar wind and radiation of the SN progenitor and other nearby massive stars.

in the articles (see Table 2). For example, AD 0185 evolved within a progenitor's wind bubble, resulting in a reduced ISM density in the vicinity of the initial SN. However, this density then experiences a sudden increase after a certain distance. These variations in the ISM were not factored into the simulations conducted in this study.

3 Summary and Conclusion

First summary the whole work – briefly repeat its aims and purpose. As a purpose, also add that the intention also was to get insights in how simulations in astronomy work in general and which research methods are used.

Then briefly repeat what exactly you did.

Regarding the conclusions you can write something like the following:

The work contributed to better understanding to how the two modules take into account different properties and affect the simulations of the SRN evolution. The results revealed that, as expected, the differences start to appear only at the later stage of SRN evolution, specifically around the transition between the Sedov-Taylor to the Pressure-Driven-Shell phase. The analyses of the simulations have shown that the effect of the two modules manifests itself as a difference in how they treat the high increase of mass preceding the shell collapse. While Schure cooling module adds the mass behind the shock front, the chemistry cooling module adds the mass onto the shock front.

Both simulations also treat differently the final stages of the SRN evolution. The chemistry cooling module simulates it in a cone shape, while the Schure cooling module simulates it in a form of two density spikes with an area of lower density in between. The difference manifests itself in size irregularities in the simulation with the Schure cooling module, because the code sometimes mistakes the first spike for the shock front and thus the actual size of the SNR

It was not possible to make conclusions about which of the simulations using the two cooling modules better fits reality due to the lack of sufficient amount of representative data about existing SRNs. However, since new data in astronomy accumulates very fast due to the advances in technology, it can be assumed that a continuation research might be possible at later time.